

Time Averaging of Chaotic Spatiotemporal Wave Patterns

B. J. Gluckman, P. Marcq,* J. Bridger, and J. P. Gollub

Physics Department, Haverford College, Haverford, Pennsylvania 19041
and Physics Department, University of Pennsylvania, Philadelphia, Pennsylvania 19104
 (Received 8 February 1993)

Chaotic spatiotemporal patterns can have highly ordered time averages. This fact is demonstrated for Faraday waves by averaging shadowgraph images. The averages exhibit box quantization effects, and their spatial form is similar to that predicted for patterns near onset, despite the large fluctuations. Patches of the disordered instantaneous patterns retain significant phase coherence with the ordered averages.

PACS numbers: 47.52.+j, 47.35.+i, 47.54.+r

A number of recent investigations have explored the properties of nonlinear hydrodynamic systems that exhibit spatiotemporal chaos, with strong fluctuations in one or two space dimensions and time [1]. Such spatially chaotic regimes are characterized by correlation lengths shorter than the system size.

Given the complexity of these nonlinear regimes, statistical rather than deterministic methods have often been used for experimental characterization [2–4]. One of the simplest statistical measures is the time average of the fluctuating pattern. This quantity has not been studied carefully, perhaps because it was presumed to be featureless in relatively large chaotic systems, or because long-term averages are sometimes hard to obtain.

Motivated by a suggestion due to Golubitsky [5], we have investigated the behavior of time averages of chaotic wave patterns produced by the Faraday instability in moderately large fluid layers [1]. We find that strikingly regular time-averaged patterns are produced well into the spatiotemporally chaotic regime. Their functional form is closely related to the product wave functions predicted near the wave onset (though with a different wave number), despite the large fluctuations present for strong excitation. Although the ordered time average would disappear for sufficiently large layers, the experiments show that the chaotic wave patterns have a high degree of phase rigidity. Possibly related phenomena include the persistence of Taylor vortices within turbulent Taylor-Couette flow [6] and the average properties of viscous fingering patterns [7].

The experiments were performed primarily in a square container, with limited measurements in circular ones. The square cell has horizontal side $L_1=8$ cm, is 2 cm high, and is half filled with *n*-butanol, a fluid that wets the Plexiglas sidewalls neatly. We refer to these boundary conditions as “wetting.” For some measurements, we have used “brim-full” or pinning boundary conditions [8] by installing a step in the cell; this reduces the interior dimensions to $L_2=6.5$ cm, without changing any of the essential phenomena, though the chaotic time dependence is somewhat slower in that case. The cell is mechanically coupled to an electromagnetic shaker in a way that allows light to pass through the fluid layer vertically for shadow-

graph visualization. Vibration frequencies $f_0=50$ –120 Hz are typical; these correspond to fluid wavelengths of 0.37–0.73 cm. The frequency-dependent critical vibration amplitude a_c is in the range 18–33 μm .

Refraction by the interface produces a shadowgraph image above the fluid surface and this image is transferred to the detector of a charged coupled device (CCD) camera by suitable optics [9]. The integration time of the CCD is sufficient to average the patterns over one or two full cycles of the waves, which oscillate at half the driving frequency. (For low driving frequencies, additional digital averaging is needed after acquisition at 30 Hz.) Because of a small optical asymmetry between the intensity fields generated at opposite phases of the standing waves, these images $I(\mathbf{r},t)$ do not vanish. They are instead closely related [10] to the *square* of the spatial part of the surface displacement field $\zeta(\mathbf{r},t)$. They accurately reveal the symmetry and periodicity of the instantaneous waves, *but with an apparent wavelength equal to exactly half the underlying fluid wavelength* λ . We refer to these as “instantaneous images,” though they are in fact averaged over one or two wave cycles, a time that is short compared to the time scale for local pattern fluctuations.

An example of such an instantaneous image $I(\mathbf{r},t)$ in the chaotic regime is shown in Fig. 1(a) at $\varepsilon=1.5$ and $f_0=120$ Hz, where $\varepsilon\equiv(a-a_c)/a_c$. The dark spots in the image correspond to antinodes of the wave pattern because the images have been digitally inverted. The pattern fluctuates rapidly; individual cells form, merge, travel, and change orientation. The time scale for local pattern fluctuations, determined from the inverse of the second moment of the local light intensity spectrum, is $\tau_l=0.7$ s.

We characterize the instantaneous images by a one-dimensional cut through the spatial autocorrelation function, averaged over a few images to improve the statistics. This quantity [11], shown in Fig. 1(b), reveals an oscillatory tail that is well approximated by the product of a cosine and a decaying exponential, once the central peak is removed by subtraction of a running average. (The central peak is augmented by imaging artifacts and is not relevant to understanding the degree of disorder.) The measured correlation length of 1.3 cm is about $7(\lambda/2)$ or

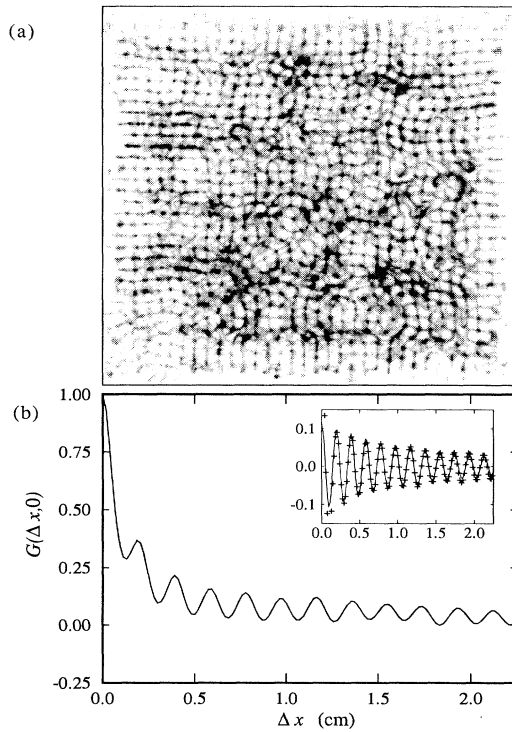


FIG. 1. (a) Image $I(\mathbf{r}, t)$ of instantaneous wave pattern in the chaotic regime; the driving frequency is $f_0 = 120$ Hz, the nondimensional driving amplitude is $\varepsilon = 1.5$, and brim-full boundary conditions are used. (b) Ensemble average of the image autocorrelation function $G(\Delta x, \Delta y)$, computed over the center half of the container area, and plotted along Δx with $\Delta y = 0$. The inset shows a fit to the tail (see text).

20% of the container width. It declines slowly with increasing ε , varying by less than a factor of 2 over the range $0.5 < \varepsilon < 3$ for brim-full boundary conditions. For wetting boundary conditions, the correlation length is a factor of 2–3 smaller.

The corresponding time-averaged image $A(\mathbf{r}) \equiv \overline{I(\mathbf{r}, t)}$ [Fig. 2(a)] has almost perfect periodicity and square symmetry. The averaged image is approximately the same (except for the wavelength halving mentioned above) as the function that would be obtained by stroboscopic sampling followed by time averaging of the actual pattern $\zeta(\mathbf{r}, t)$. The example shown was averaged over 1100 s, but the result is not sensitive to the duration, provided the averaging time is long compared to τ_l . Our experiments also allow us to determine conclusively that waves driven at f_0 by the sidewalls rather than at $f_0/2$ by the Faraday instability are *not* the cause of the nonzero averages.

To better understand this averaged chaotic pattern, we pose the following question: What space- and time-periodic surface height variation $\zeta(\mathbf{r}, t)$ would give rise to it? If we choose axes aligned with the container boundaries (and with the origin at one of its corners), then the

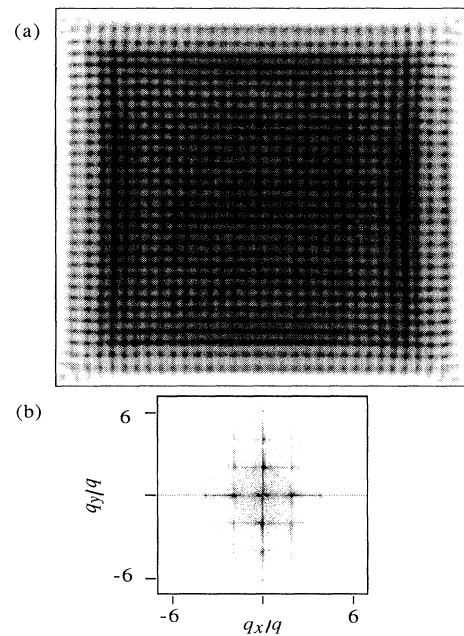


FIG. 2. (a) Time-averaged image $A(\mathbf{r}) \equiv \overline{I(\mathbf{r}, t)}$ (over 1100 s) under the same conditions as in Fig. 1. (b) Spatial power spectrum of the center fourth of the average. The forms of the image and its spectrum are similar to those that would be produced by a pure product mode $\zeta_1(x, t)$ with wave number $q = 16.3 \text{ cm}^{-1}$.

obvious candidate (with pinning boundary conditions that force the displacement to vanish) is a product wave function $\zeta_1(x, y, t) \sim (\sin qx)(\sin qy) \sin \pi f_0 t$. The spatial power spectrum, shown in Fig. 2(b), is consistent with this form. For example, the experimental pattern has dominant spectral peaks at $2q\hat{x}$, $2q\hat{y}$, and $2q\hat{x} + 2q\hat{y}$. (Recall that the factor of 2 results from the imaging process.) To confirm this interpretation, we have also performed extensive ray tracing computations of the shadowgraph images and corresponding spatial power spectra, assuming $\zeta_1(x, y, t)$. We find semiquantitative agreement between the computed and observed patterns in the bulk of the cell, and similarly for the spectra. [We note parenthetically that an alternate form $\zeta_2(x, y, t) \sim (\sin qx + \sin qy) \sin \pi f_0 t$ is predicted *close to onset* and has been observed *away from boundaries* in other experiments at higher frequencies [10].]

Thus, the averaged chaotic pattern in the central region of the cell has approximately the form of the pure modes expected near onset in a square container. There is some additional structure near the side walls. (However, the *actual* patterns obtained near onset are often not pure modes; symmetrized superpositions of two modes with different mode numbers along x and y are generally obtained [8].)

How does the degree of order in the time average depend on driving amplitude ε ? We display in Fig. 3 the

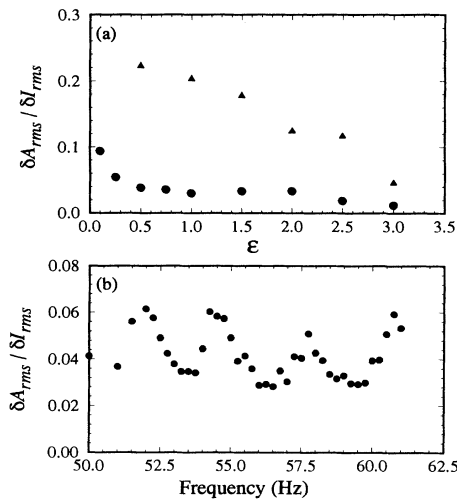


FIG. 3. (a) Root-mean-square amplitude δA_{rms} of the average pattern, normalized by the corresponding value δI_{rms} for instantaneous patterns, as a function of nondimensional driving amplitude, with $f_0 = 120$ Hz: Δ , brim-full boundary conditions; \circ , wetting boundary conditions. (b) Dependence of δA_{rms} on driving f_0 for the wetting case at $\varepsilon = 1.5$; the average is more pronounced at certain frequencies.

rms variation of the time average, δA_{rms} , normalized by the corresponding rms variation δI_{rms} of instantaneous images at the same value of ε . These quantities are defined by the expressions $\delta A_{rms} = \langle [A(\mathbf{r}) - \langle A \rangle]^2 \rangle^{0.5}$ and $\delta I_{rms} = \langle [I(\mathbf{r}, t) - \langle I \rangle]^2 \rangle^{0.5}$, where brackets denote *spatial* averages. However, even the second of these is effectively time independent. Measurements are shown for both brim-full and wetting boundary conditions. The brim-full case where the meniscus is pinned gives the larger amplitude, though both are well above the measurement noise. In both cases, δA_{rms} declines with increasing ε , though rather large amplitudes are required to eliminate the structure in the average pattern. The rms amplitude of the average pattern is also frequency dependent. We find [Fig. 3(b)] a pronounced periodicity in δA_{rms} but not in δI_{rms} .

Now we come to the problem of “pattern selection” in the chaotic regime. What is the wave number q of the averaged patterns? We measured it as a function of driving frequency, and the result is shown in Fig. 4(a). We see that the averaged patterns exhibit finite size quantization; each step corresponds to a fixed integer number N of half wavelengths; several of these integers are noted in the figure. It is remarkable that this quantization effect is so strong in the behavior of the averaged chaotic patterns, despite the short correlation time for pattern rearrangements. Furthermore, we note that the minima in δA_{rms} noted in Fig. 3(b) coincide with the transitions between steps in Fig. 4(a).

It is of interest to compare the measured wave number q with the value k given by the dispersion relation,

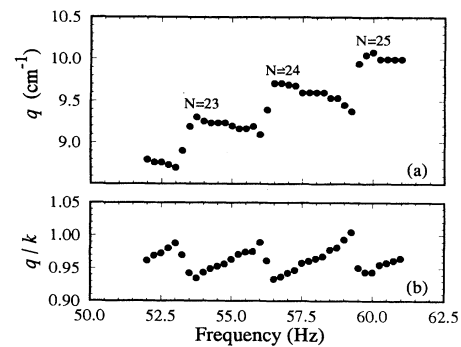


FIG. 4. (a) Mean wave number of the average pattern as a function of driving frequency at $\varepsilon = 1.5$, and with wetting boundary conditions. The steps indicate that phase coherence is maintained despite large chaotic fluctuations. (b) Ratio of the measured (one-dimensional) wave number to that computed from the dispersion relation.

$\omega^2 = (gk + \gamma k^3/\rho) \tanh kh$, where $\omega = \pi f_0$, γ is the surface tension, ρ is the fluid density, and the factor depending on the depth h is close to unity at the wavelengths of interest. The ratio q/k of the measured (one-dimensional) wave number to the value given by the dispersion relation is shown in Fig. 4(b). It is close to unity, except for the distortion caused by “mode pulling” to the cavity. Though this result $q/k \approx 1.0$ appears to be natural, it is in fact somewhat surprising. The analogy to patterns near onset (as suggested by the wave forms) leads us to expect the ratio $\sqrt{2}q/k$ to be unity instead, since the wave numbers along x and y would be added in *quadrature* for a product wave form. Thus, the wave number selection *does not* match that expected for patterns near onset, nor should it necessarily be expected to do so.

We have also investigated the *dynamics* of the fluctuations of the instantaneous patterns. One can imagine several possible scenarios leading to ordered average patterns: (a) The instantaneous patterns occasionally pass through states very close to the average, and possibly remain there for relatively long times. (b) Patterns fluctuate randomly, but are biased toward the average pattern, perhaps because patches are close to the average.

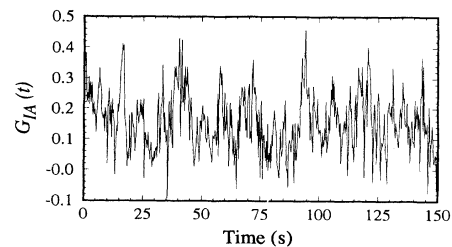


FIG. 5. Time-dependent cross-correlation coefficient (see text) between instantaneous patterns and the average, for $\varepsilon = 1.5$ and $f_0 = 120$ Hz using brim-full boundary conditions. The fluctuations are approximately Gaussian.

Some insight into the dynamics can be obtained by examining the time-dependent cross-correlation coefficient $G_{IA}(t)$ between instantaneous and averaged images. This quantity is defined as $G_{IA}(t) = \langle \delta I(\mathbf{r}, t) \delta A(\mathbf{r}) \rangle / I_{\text{rms}} A_{\text{rms}}$. We utilize the center fourth of the container area to avoid wall effects, and examine a time series consisting of 500 images spaced 0.3 s apart. This quantity is shown in Fig. 5. We find that the mean correlation is about 0.16, the standard deviation is about 0.10, and some patterns are anticorrelated with the average pattern. The fluctuations of $G_{IA}(t)$ are not far from Gaussian, and no events with correlations above 0.5 are found. The characteristic time scale of the pattern fluctuations [determined from the spectrum of $G_{IA}(t)$] is about 2.2 s, somewhat longer than the local fluctuation time τ_l mentioned earlier.

These observations imply that scenario (b) is more nearly correct: There is no evidence that states very close to the average pattern occur. Rather, the ordered average is obtained because the instantaneous patterns have short-lived patches [Fig. 1(a)] of size comparable to the correlation length that are regular and spatially in phase with the average. After the completion of this work, we became aware of another experiment on Faraday waves, now published, in which intermittent wave patches manifest long range, but in that case algebraically decaying, correlations [12]. However, the two experiments should be compared with caution, as the fluid viscosities are very different.

In this study of some of the statistical properties of spatiotemporally chaotic Faraday waves, we found surprisingly ordered time-averaged patterns [Fig. 2(a)] in the presence of large fluctuations, and have determined the selected pattern quantitatively. The effect persists far into the chaotic regime, where individual patterns are relatively disordered except at the walls. The effect is substantial in containers that are moderately large ($\approx 30\lambda/2$), though it would presumably vanish when the size is increased sufficiently. Its magnitude is influenced by the sidewall boundary conditions, and appears to be related to the correlation length of the instantaneous patterns.

We have conducted more limited experiments in a cir-

cular cell of comparable size. In this case the average pattern shows rings similar to the linear modes of a circular container. A fuller investigation of the dynamics of the fluctuations and the effects of container symmetry will appear elsewhere.

This work was supported primarily by NSF Grant No. DMR-8901869, with additional support from CTS-9115005. We appreciate helpful discussions with M. Golubitsky, who brought to our attention the problem of the symmetry of averaged patterns. We also acknowledge helpful discussions with S. Edwards, P. Hohenberg, and B. Shraiman.

*Currently at SPEC, CEN Saclay, 91191 Gif sur Yvette Cedex, France.

- [1] M. C. Cross and P. C. Hohenberg, *Rev. Mod. Phys.* (to be published).
- [2] S. Ciliberto and P. Bigazzi, *Phys. Rev. Lett.* **60**, 286 (1988); M. Caponeri and S. Ciliberto, *Physica (Amsterdam)* **58D**, 365 (1992).
- [3] N. B. Tufillaro, R. Ramshankar, and J. P. Gollub, *Phys. Rev. Lett.* **62**, 422 (1989).
- [4] M. Dubois, F. Daviaud, and M. Bonettie, *Phys. Rev. A* **42**, 3388 (1990).
- [5] M. Golubitsky (private communication); see also P. Chossat and M. Golubitsky, *Physica (Amsterdam)* **32D**, 423 (1988).
- [6] D. P. Lathrop, J. Fineberg, and H. L. Swinney, *Phys. Rev. Lett.* **68**, 1515 (1992).
- [7] A. Arnéodo, Y. Couder, G. Grasseau, V. Hakim, and M. Rabaud, *Phys. Rev. Lett.* **63**, 984 (1989).
- [8] S. Douady and S. Fauve, *Europhys. Lett.* **6**, 221 (1988).
- [9] W. Merzkirch, *Flow Visualization* (Academic, Orlando, 1987).
- [10] J. P. Gollub and R. Ramshankar, in *New Perspectives in Turbulence*, edited by L. Sirovich (Springer-Verlag, New York, 1991), p. 165.
- [11] The autocorrelation function $G(\Delta x, \Delta y)$ of the instantaneous images is computed from fluctuations with respect to the time average $A(\mathbf{r}) \equiv \overline{I(\mathbf{r}, t)}$, so that it can be expected to vanish for large displacements.
- [12] E. Bosch and W. van de Water, *Phys. Rev. Lett.* **70**, 3420 (1993).

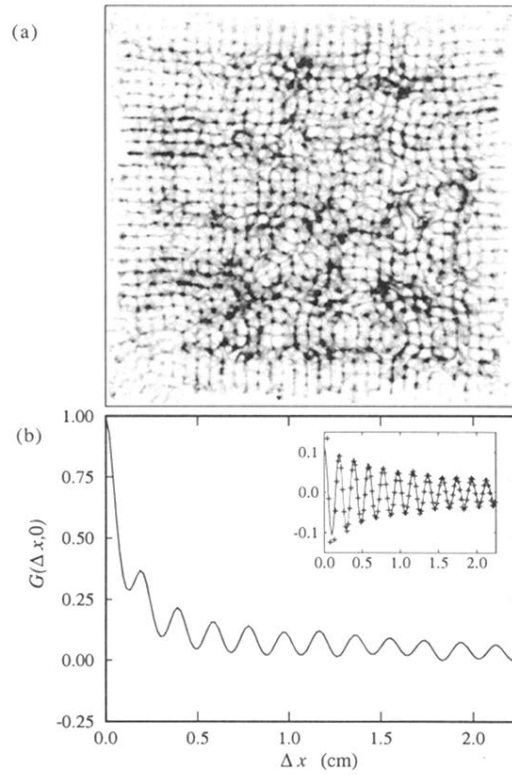


FIG. 1. (a) Image $I(\mathbf{r}, t)$ of instantaneous wave pattern in the chaotic regime; the driving frequency is $f_0 = 120$ Hz, the nondimensional driving amplitude is $\varepsilon = 1.5$, and brim-full boundary conditions are used. (b) Ensemble average of the image autocorrelation function $G(\Delta x, \Delta y)$, computed over the center half of the container area, and plotted along Δx with $\Delta y = 0$. The inset shows a fit to the tail (see text).

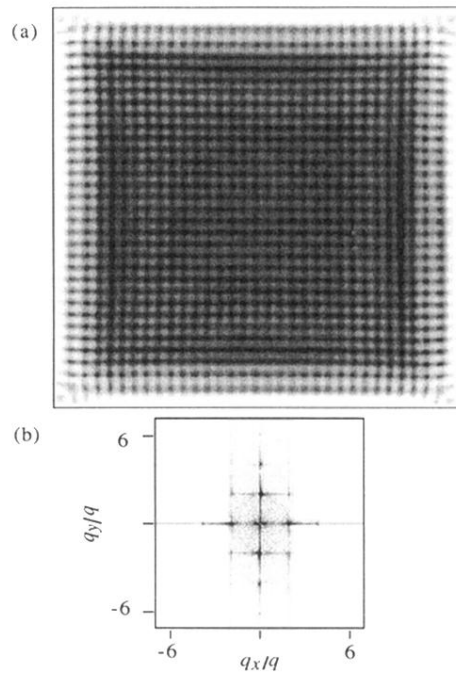


FIG. 2. (a) Time-averaged image $A(\mathbf{r}) \equiv \overline{I(\mathbf{r}, t)}$ (over 1100 s) under the same conditions as in Fig. 1. (b) Spatial power spectrum of the center fourth of the average. The forms of the image and its spectrum are similar to those that would be produced by a pure product mode $\zeta_1(x, t)$ with wave number $q = 16.3 \text{ cm}^{-1}$.